Thermal Models of a TN-32B Cask for the International Benchmark

Spent Fuel and Waste Disposition

Prepared for
US Department of Energy
Spent Fuel and Waste Science and Technology

JA Fort
DJ Richmond
BJ Jensen

October 23, 2020
PNNL-30645

SUMMARY

The Spent Fuel and Waste Science and Technology (SFWST) research and development (R&D) program of the U.S. Department of Energy is conducting a high burnup fuel storage demonstration for a storage module in the North Anna Nuclear Power Station's Independent Spent Fuel Storage Installation (ISFSI). The storage module selected for this demonstration is an Orano TN-32B High Burnup cask. The main goals of this test are to provide confirmatory data for model validation and potential improvement, support license renewals and new licenses for ISFSIs, and support transportation licensing for high burnup spent nuclear fuel (EPRI 2014). The focus of the Demonstration test is the performance of the high burnup fuel.

A round robin thermal modeling exercise was conducted around the loading to compare predictions with measurements (EPRI 2020a). The participants used proprietary data as inputs. There was significant interest from the broader community in a similar modeling exercise. The Electric Power Research Institute (EPRI) agreed to host a follow up International Benchmark and worked with PNNL and Orano to produce a set of non-proprietary inputs for use by participants. The first meeting was held with participants and observers on April 28, 2020. Some participants plan to have results ready for the fall Extended Storage Collaboration Program (ESCP) meeting in November. The remainder will submit results in time for publication of the collected model results in 2021.

PNNL is also participating in this exercise by adapting models used in the proprietary exercise with the new inputs for the International Benchmark. The purpose of the PNNL modeling in this exercise is to provide a comparison of PNNL modeling with and without the proprietary data. Results for the PNNL models using proprietary inputs are described in Fort et al (2019a). Results for three models are reported in this document. In each case the model compared favorably to the data and the previous modeling conducted with proprietary design information. These results verify the adequacy of the International Benchmark specifications and any model comparisons that are conducted with this dataset.

THIS PAGE INTENTIONALLY LEFT BLANK.

ACKNOWLEDGEMENTS

PNNL wishes to thank the Electric Power Research Institute (EPRI) for coordinating the International Benchmark activity, in particular Hatice Akkurt and Al Csontos. We also thank Orano TN (formerly AREVA TN) for working with EPRI to review and provide approval for release of the storage cask information provided to benchmark participants. The authors appreciate the contribution of Colleen Winters for editing and formatting this document.

THIS PAGE INTENTIONALLY LEFT BLANK.

CONTENTS

THIS PAGE INTENTIONALLY LEFT BLANK.

LIST OF FIGURES

THIS PAGE INTENTIONALLY LEFT BLANK.

LIST OF TABLES

THIS PAGE INTENTIONALLY LEFT BLANK.

ACRONYMS

DOE	US Department of Energy
EPRI	Electric Power Research Institute
ESCP	Extended Storage Collaboration Program
ISFSI	independent spent fuel storage installation
NRC	Nuclear Regulatory Commission
SNF	spent nuclear fuel

THIS PAGE INTENTIONALLY LEFT BLANK.

THERMAL MODELING OF A TN-32B CASK FOR THE INTERNATIONAL BENCHMARK

1. INTRODUCTION

The Spent Fuel and Waste Science and Technology (SFWST) research and development program of the U.S. Department of Energy is conducting a high burnup fuel storage demonstration for a storage module in the North Anna Nuclear Power Station's Independent Spent Fuel Storage Installation (ISFSI). The storage module selected for this demonstration is an Orano TN-32B High Burnup cask. The main goals of this test are to provide confirmatory data for model validation and potential improvement, support license renewals and new licenses for ISFSIs, and support transportation licensing for high burnup spent nuclear fuel (EPRI 2014). The focus of the demonstration test is the performance of the high burnup fuel.

A round robin thermal modeling exercise was conducted around the time the cask was loaded to compare predictions with measurements (EPRI 2020a). The participants used proprietary data to inform model inputs. Based on the results of this exercise there was a significant interest from outside organizations in modeling the same cask using non-proprietary design information. This activity is termed the International Benchmark and the Electric Power Research Institute (EPRI) agreed to host it through the Extended Storage Collaboration Program (ESCP) program. They worked with PNNL and Orano to produce a set of non-proprietary inputs for use by participants. The first meeting was held with participants and observers on April 28, 2020. Participants agreed to try and have results ready for the Winter ESCP meeting in November 2020.

To provide confirmation that the non-proprietary inputs will produce the expected results, PNNL has updated the two models used in the proprietary round robin with new inputs for the International Benchmark. The two models in the proprietary round robin were developed using COBRA-SFS (Michener et al 2017) and STAR-CCM+ (Siemens 2020). The STAR-CCM+ model used a porous media representation of the fuel. This report presents the results from the updated COBRA-SFS and STAR-CCM+ porous models as well as a STAR-CCM+ model with a detailed representation of the fuel.

The problem statement for the International Benchmark was provided to participants (EPRI, 2020b). A summary of that problem statement is provided in Section 2 of this report. Section 3 describes the changes that were made to each of the PNNL models for agreement with the benchmark. Section 4 presents model results and includes a discussion of the model differences and similarities. Section 5 lists conclusions and recommendations and Section 6 contains the report references.

THIS PAGE INTENTIONALLY LEFT BLANK.

2. PROBLEM DEFINITION

As in the initial round robin exercise, the objective was to obtain steady state temperatures achieved during the two-week thermal soak period in the North Anna decontamination bay. The problem definition provided to participants builds on the description of the High Burnup Demonstration thermal soak that was included as Appendix A in Fort et al (2019a). This section of the report summarizes the changes made to that description to provide modeling participants with an adequate description of the cask and conditions, as well as a common set of inputs and boundary conditions for ease of comparing submitted model results.

2.1 Cask Geometry

PNNL prepared simplified drawings of the TN-32B cask that would be sufficient for thermal modeling. These drawings were submitted to Orano TN for review and their requested modifications were implemented in the final drawing set. The finalized drawings were then made available to International Benchmark participants. These drawings are included in the problem statement (EPRI, 2020b). The STAR-CCM+ porous model geometry developed from these drawings is shown in Figure 1 and the detailed model in Figure 2.

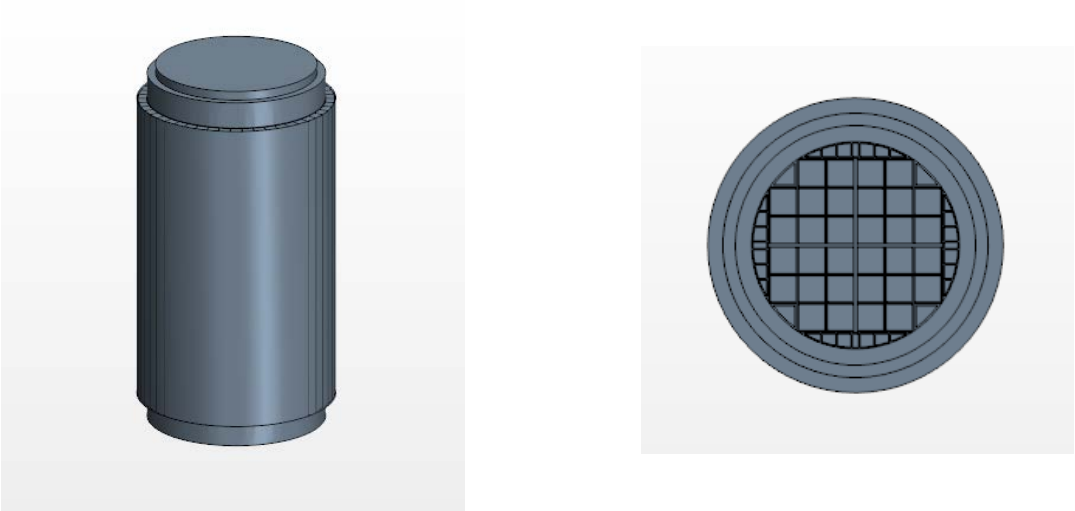

Figure 1. TN-32B Cask Geometry as Represented in STAR-CCM+ Porous Model

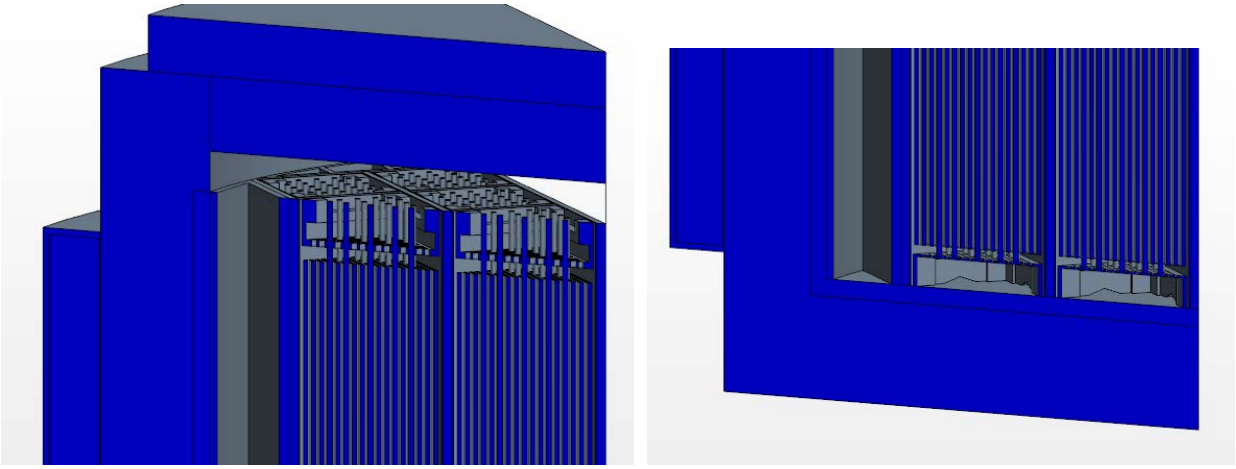

Figure 2. One-eighth Section TN-32B Cask Geometry as Represented in STAR-CCM+ Detailed Model

2.2 Cask Materials

The TN-32B is a metal cask with liner, lid, and gamma shield made from carbon steel. The radial neutron shield surrounds the cylindrical body of the cask and is enclosed in a carbon steel shell. The radial neutron shield consists of borated polyester resin enclosed in full-length aluminum box sections. Materials for cask components are included in the drawing set in EPRI 2020b and are listed here in Table 1.

Table 1. TN-32B Cask Materials

Component	Material
Lid	SA-350 G LF3, or SA 203 Gr A or D
Top shield plate	SA 105 or SA 516 Gr 70
Inner liner/containment	SA 203 Gr A
Gamma shield	SA 516 Gr 70
Outer shell	SA 516 Gr 70
Basket fuel compartments	SA 240 Type 304
Basket plates	6061 T6
Poison plates	Borated aluminum
Radial neutron shield box	6063 T5
Basket transition rails	6061 T6
Radial neutron shield	Borated polyester resin

Surface coatings are applied to the cask interior and to the cask exterior. The cask cavity is spray coated with aluminum for corrosion protection. The exterior of the cask is coated with epoxy paint.

2.3 Material Properties

Cask material properties are provided in Table 2. Surface properties are listed in Table 3.

Table 2. Material Properties

Material	Density, kg/m3	Specific Heat, J/kg-K	Thermal Conductivity, W/m-K			
			300 K	400 K	600 K	800 K
Carbon steel SA 203 Gr A[a]	7817	434	51.9	49.8	44.0	37.4
Carbon steel SA 516 Gr 70[b]	7854	434	60.5	56.7	48.0	39.2
Aluminum 6061 T6[c]	2700	903	167			
Aluminum 6063 T5[d]	2700	903	209			
Stainless steel AISI 304	7900	477	14.9	16.6	19.8	22.6
Polyester resin[e]			0.18			

[a] Incropera (2007) properties for carbon-silicon steel
[b] Incropera (2007) properties for plain carbon steel
[c] www.gabrian.com/wp-content/uploads/2018/09/6061-Aluminum-Alloy-Properties-1.pdf
[d] www.gabrian.com/wp-content/uploads/2018/09/6063-Aluminum-Alloy-Properties.pdf
[e] N.W. Pech-May et al./Polymer Testing 50 (2016) 255e261

Table 3. Emissivities of Cask Materials

Material	Emissivity
Carbon steel	0.45
Aluminum	0.2
Stainless steel	0.3
Aluminum spray coating	0.2
Painted exterior	0.9

2.4 Cask Component Gaps

Thermal gap resistances are included in the models. The component pairs and associated gap distances are listed in Table 4. The gas filling these gaps is helium, unless specified otherwise.

Table 4. Assumptions for Component Gap Spacing (helium filled, except where noted)

Component Pair	Gap, Inches
Basket plate ends	0.02
Basket corners to cask inner liner	0.2
Transition rail to basket	0.1
Transition rails to cask inner liner	0.01
Cask inner liner to radial gamma shield	Interference fit
Cask inner liner to base gamma shield	0.125 (air)
Fuel compartment to basket plate	0.02
Radial neutron shield box to gamma shield	0.01
Radial neutron shield box to outer shell	0.01

2.5 Fuel Geometry and Decay Heat

The loading map for the demonstration cask is shown in Figure 3. Included in each basket location is the fuel assembly type and estimated decay heat at the time of loading. Total estimated decay heat for this November 2017 loading was 30.46 kW.

Fuel rod diameters for each fuel type are specified in the problem statement (EPRI 2020b) along with axial position of the start of active length. Axial power profile is also provided in the problem statement. That profile was the average for all fuel assemblies. For additional fuel assembly geometry, the participants are to use properties for Westinghouse 17x17.

	1 6T0 NAIF/P+Z Zirlo, 54.2 GWd 4.25%/3 cy/12.1 yr 912.2 W	2 (TC Lance) 3K7 AMBW M5, 53.4 GWd 4.55%/3 cy/8.7 yr 978.2 W	3 3T6 NAIF/P+Z Zirlo, 54.3 GWd 4.25%/3 cy/12.1 yr 914.4 W	4 6F2 NAIF/P+Z Zirlo, 51.9 GWd 4.25%/3 cy/13.5 yr 799.5 W	Drain Port
5 3F6 NAIF/P+Z Zirlo, 52.1 GWd 4.25%/3 cy/13.5 yr 800.9 W	6 (TC Lance) 30A AMBW M5, 52.0 GWd 4.55%/3 cy/7.2 yr 1008.6 W	7 22B AMBW M5, 51.2 GWd 4.55%/3 cy/5.7 yr 1142.4 W	8 (PRA) 20B AMBW M5, 50.5 GWd 4.55%/3 cy/5.7 yr 1121.2 W	9 5K6 AMBW M5, 53.3 GWd 4.55%/3 cy/8.7 yr 975.1 W	10 5D5 NAIF/P+Z Zirlo, 55.5 GWd 4.20%/3 cy/17.7 yr 814.5 W
11 (Vent Port) 5D9 NAIF/P+Z Zirlo, 54.6 GWd 4.20%/3 cy/17.7 yr 802.6 W	12 28B AMBW M5, 51.0 GWd 4.55%/3 cy/5.7 yr 1135.0 W	13 (PRA) F40 LOPAR Zry-4, 50.6 GWd 3.59%/3 cy/30.6 yr 573.8 W	14 (TC Lance) 57A AMBW M5, 52.2GWd 4.55%/3 cy/7.2 yr 1037.0 W	15 (PRA) 30B AMBW M5, 50.6 GWd 4.55%/3 cy/5.7 yr 1124.8 W	16 3K4 AMBW M5, 51.8 GWd 4.55%/3 cy/8.7 yr 941.3 W
17 5K7 AMBW M5, 53.3 GWd 4.55%/3 cy/8.7 yr 961.7 W	18 (PRA) 50B AMBW M5, 50.9 GWd 4.55%/3 cy/5.7 yr 1131.1 W	19 (TC Lance) 3U9 NAIF/P+Z Zirlo, 53.1 GWd 4.45%/3 cy/10.6 yr 920.2 W	20 (PRA) 0A4 NAIF Low-Sn Zry-4, 50.0 GWd 4.00%/2 cy/23.2 yr 646.2 W	21 15B AMBW M5, 51.0 GWd 4.55%/3 cy/5.7 yr 1135.8 W	22 6K4 AMBW M5, 51.9 GWd 4.55%/3 cy/8.7 yr 941.2 W
23 3T2 NAIF/P+Z Zirlo, 55.1 GWd 4.25%/3 cy/12.1 yr 934.7 W	24 (TC Lance) 3U4 NAIF/P+Z Zirlo, 52.9 GWd 4.45%/3 cy/10.6 yr 914.2 W	25 (PRA) 56B AMBW M5, 51.0 GWd 4.55%/3 cy/5.7 yr 1133.7 W	26 54B AMBW M5, 51.3 GWd 4.55%/3 cy/5.7 yr 1136.3 W	27 6V0 AMBW M5, 53.5 GWd 4.40%/3 cy/8.7 yr 988.2 W	28 (TC Lance) 3U6 NAIF/P+Z Zirlo, 53.0 GWd 4.45%/3 cy/10.6 yr 916.9 W
	29 4V4 AMBW M5, 51.2 GWd 4.40%/3 cy/9.1 yr 914.2 W	30 5K1 AMBW M5, 53.0 GWd 4.55%/3 cy/8.7 yr 968.0 W	31 (TC Lance) 5T9 NAIF/P+Z Zirlo, 54.9 GWd 4.25%/3 cy/12.1 yr 927.7 W	32 4F1 NAIF/P+Z Zirlo, 52.3 GWd 4.25%/3 cy/13.5 yr 804.3 W	

Figure 3. Assembly Loading Map

2.6 Effective Properties for the Fuel

Porous media models require effective properties for flow resistance and for effective thermal conductivity, including thermal radiation. References for available values are provided in the problem statement (EPRI 2020b). Flow resistances for the fuel assemblies are to be used from Section 5.3.1 of Fort et al (2016). Axial fuel effective thermal conductivity is listed as Eq. 5.3 of Fort et al (2016) and radial effective thermal conductivity is given as a curve fit in Figure 2-12 of Fort et al (2019a). All these values were calculated for the Westinghouse 17x17 Optimized Fuel Assembly (WE 17x17 OFA).

2.7 Boundary Conditions

Boundary conditions are natural convection and thermal radiation from all surfaces. Since the cask was supported off the floor, this treatment also applied to the cask bottom. A uniform average ambient temperature of 75°F is to be used along with length scales from the drawings in EPRI 2020b and natural convection correlation for the surface as shown in in Table 5.

Table 5. Natural Convection Correlations (from Heat Transfer by J.P. Holman 1996)

Heated Surface	**Laminar**	**Turbulent**
	$10^4 < GrPr < 10^9$	$GrPr > 10^9$
Vertical plane or cylinder	$h = 1.42(\Delta T/L)^{1/4}$	$h = 1.31(\Delta T)^{1/3}$
Horizontal plate facing upward	$h = 1.32(\Delta T/L)^{1/4}$	$h = 1.52(\Delta T)^{1/3}$
Horizontal plate facing downward	$h = 0.59(\Delta T/L)^{1/4}$	-

THIS PAGE INTENTIONALLY LEFT BLANK.

3. MODEL UPDATES

The models used in the initial round robin modeling exercise are described in Fort et al. (2019a). The changes required by the problem statement fall into these categories:

- Cask geometry
- Material properties
- Flow loss coefficients

The cask geometry changes were relatively minor, but necessary to protect proprietary information. The difference in material properties mainly involved specifying different material properties for the carbon steel components. For the porous model, flow loss coefficients were specified for a publicly available Westinghouse 17x17 fuel assembly design as described in Section 3.1, below. The other two models (Sections 3.2 and 3.3) used an explicit representation of the fuel hardware to compute flow losses.

3.1 STAR-CCM+ Porous Model

Small changes to the cask geometry allowed mesh settings to be kept unchanged. Therefore, mesh convergence studies done previously still apply (see Section 5.1.2.5 of Fort et al 2019a). After geometry, the most significant change in this model was to incorporate flow loss coefficients for the WE 17x17 OFA fuel assemblies. Geometry for this fuel can be found in DOE (1992), DOE (1981) and development of the loss coefficients using this geometry is described in in Fort et al (2016). Material properties were changed for the carbon steel components from generic mild steel to values that were representative of ASME code values for each carbon steel type. These are specified in Table 2. Finally, boundary conditions were changed on the base of the cask. For the International Benchmark, thermal radiation and convection was applied on the cask base to a 75°F ambient.

3.2 STAR-CCM+ Detailed Model

A detailed model of the demonstration cask was not used in the proprietary round robin exercise, but one was developed for modeling the vacuum drying transient. That model was described in detail in Fort et al (2019b). It also used geometry for WE 17x17 OFA fuel, but in this case the fuel assembly is modeled explicitly, thus avoiding the need for effective fuel properties and pre-calculated flow loss coefficients. Because of its high computational cell count, only a one-eighth section of the cask was modeled (Figure 2). This detailed model was adapted for steady state calculations. It was updated with all associated geometry and input changes required for the International Benchmark. As in the case of the porous model, mesh settings were kept the same as in the original model.

3.3 COBRA-SFS Model

The COBRA-SFS model was updated in accordance with the problem statement. This consisted of minor changes to fuel geometry and materials properties as described in Section 2. The primary substantive difference was the change of the lower boundary. Previously the COBRA-SFS model used a conduction-based model that accounted for the feet of the cask leveling pad and floor of the building. This model had a boundary temperature modeled at the building foundation instead of directly on the bottom of the cask. The International Benchmark model applied the boundary temperature directly to the bottom of the leveling pad with a natural convection correlation.

THIS PAGE INTENTIONALLY LEFT BLANK.

4. MODEL RESULTS

This section presents model results for all three PNNL models. Comparisons are made with data at measurement points on the cask surface and at assembly thermocouple lance locations[a]. The steady state thermocouple data the model results are being compared against is presented in Table 6.

Table 6. Thermocouple Data (°C)

Assembly	2 (3K7)	6 (30A)	14 (57A)	19 (3U9)	24 (3U4)	28 (3U6)	31 (5T9)
Lance positions (in.)							
9	132.8	136.6	143.8	141.5	135.3	121.6	131.9
25	166.9	174.3	186.2	180.8	171.7	151.1	164.9
40	181.3	191.3	205.6	200.0	189.1	164.4	181.8
60	191.4	203.7	220.7	215.2	201.3	174.3	193.9
76	194.2	207.9	227.2	221.1	205.7	177.6	198.0
94	194.1	209.3	229.2	223.3	207.2	178.1	199.6
117	190.7	206.2	225.4	218.5	201.8	173.4	194.2
140	170.2	183.9	201.7	195.9	177.7	151.8	171.5
150	150.6	160.8	178.3	174.4	155.4	130.8	150.7

4.1 STAR-CCM+ Porous Model

Model results for measurement locations for all thermocouple lances are compared with measured data in Figure 4. The model predictions are generally higher than the measurements, but the axial profile is well represented. The magnitude of the model overpredictions can be illustrated by plotting model differences from measurements, as shown in Figure 5. The differences are greatest for the lance in assembly 28, which is on the outside of the basket and on a corner. For other thermocouple lance locations, the model predictions are all within 20°C of the measurements. Agreement is especially good at the bottommost measurement locations, within 5°C. At the uppermost measurement location, the distribution of differences is broadly distributed, ranging from +/- 8°C. Tabulated versions of model predictions and differences from measured data are provided in Table 7 and Table 8.

When compared to the STAR-CCM+ porous model for the proprietary round robin in Fort et al (2019a), the magnitude of differences from the measured temperatures at the thermocouple lance positions is improved in the present model. For the hot basket cell location (assembly 14), the present model is closer to measurements by approximately 7°C at the lowest thermocouple location and at the peak temperature location. That difference is even larger at the top thermocouple location in that cell.

How can the model using non-proprietary inputs be closer to the thermocouple measurements? It is important to point out the number of differences between the initial porous model and this one. Beyond the geometry changes to protect proprietary information, the following significant changes were made:

[a] See EPRI (2019) for these datasets.

- Thermal radiation added to the bottom boundary and a slightly higher convective heat transfer coefficient on that boundary computed using the correlation specified for this exercise.
- Thermal conduction modeled in the unheated length of the fuel rods and in the bottom spacer; in the initial model these were modeled as helium.
- More accurate thermal conductivity values for the carbon steel cask components; properties for generic carbon steel with a lower thermal conductivity was used in the initial round robin.

Taken together, the model changes are less conservative, resulting in the net improvement in model predictions.

A comparison is also made with cask surface temperature measurements that were taken using thermal imaging. The measurement locations are shown in Figure 6 and a normalized comparison with those measurements (model minus measured) is shown in Figure 7.

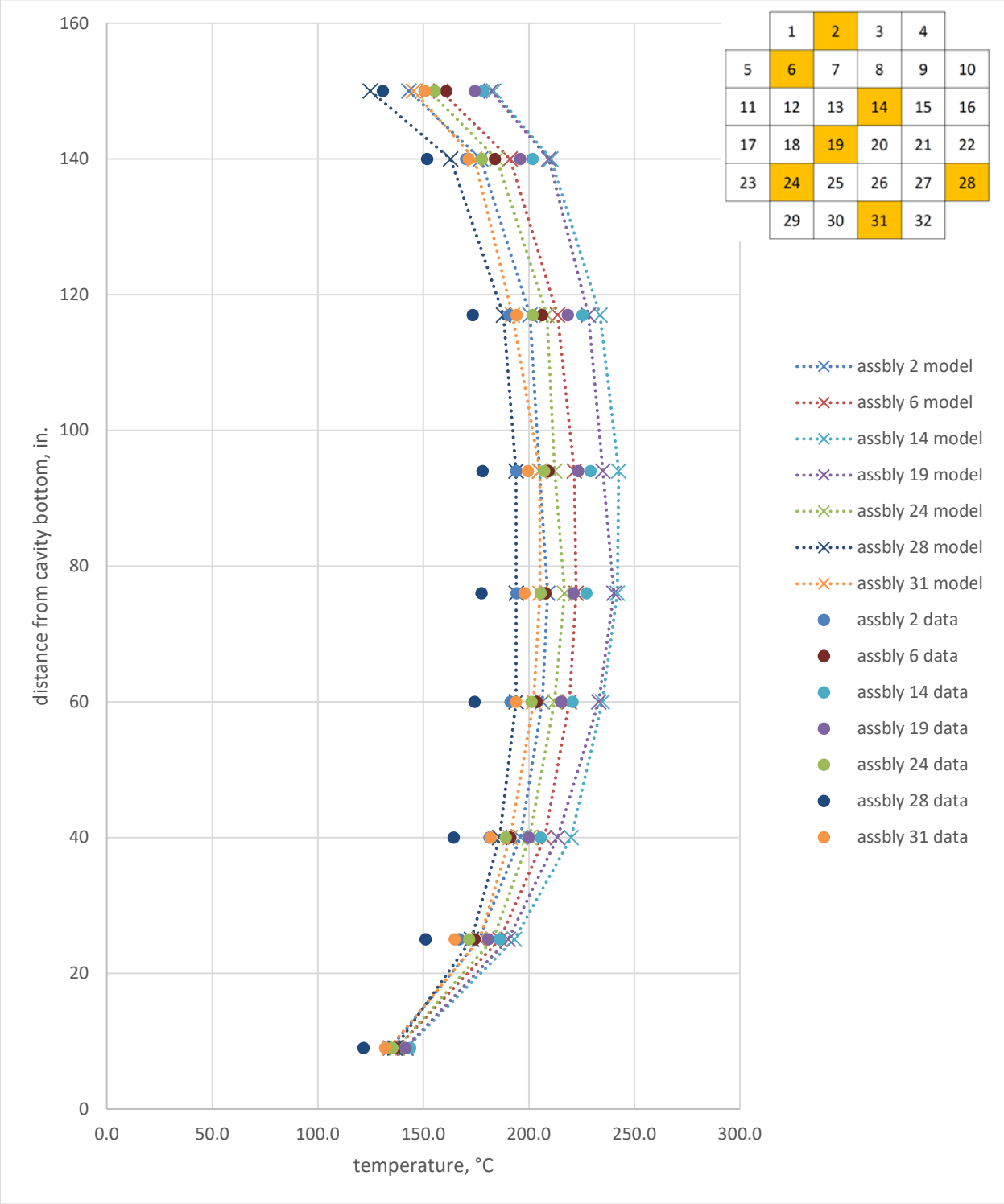

Figure 4. STAR-CCM+ Porous Model Predictions Compared to Thermocouple Measurements

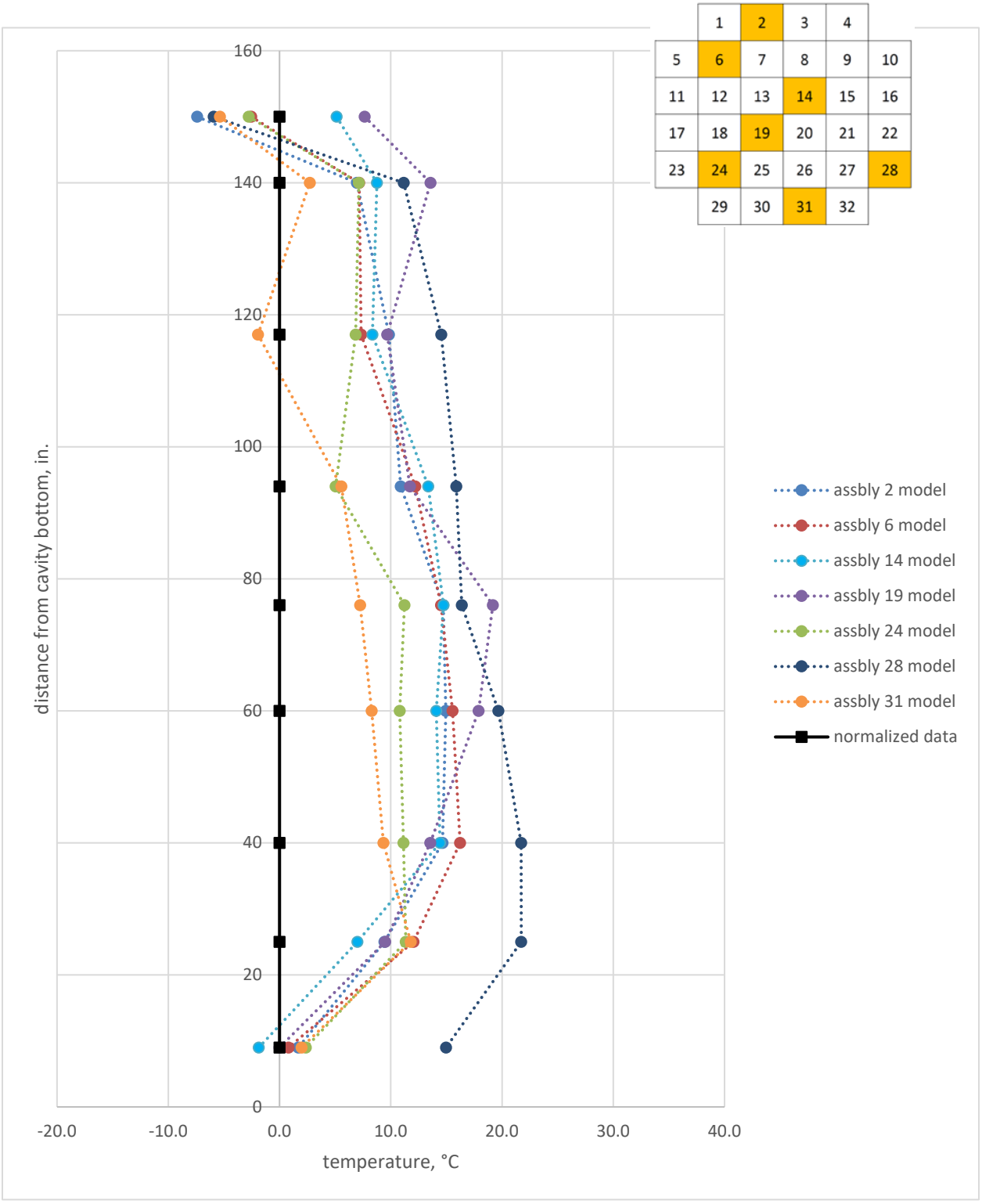

Figure 5. STAR-CCM+ Porous Model – Differences Between Predictions and Thermocouple Measurements

Table 7. STAR-CCM+ Porous Thermocouple Predictions (°C)

Assembly	2 (3K7)	6 (30A)	14 (57A)	19 (3U9)	24 (3U4)	28 (3U6)	31 (5T9)
Lance positions (in.)							
9	134.5	137.4	141.9	141.5	137.7	136.6	133.9
25	176.3	186.3	193.2	190.3	183.1	172.8	176.7
40	196.0	207.5	220.0	213.5	200.2	186.1	191.1
60	206.3	219.2	234.8	233.1	212.1	194.0	202.2
76	208.9	222.4	241.9	240.3	216.9	194.0	205.2
94	205.0	221.5	242.6	235.0	212.2	194.0	205.2
117	200.5	213.5	233.8	228.2	208.6	187.9	192.3
140	177.2	191.1	210.5	209.5	184.8	163.0	174.2
150	143.2	158.2	183.3	182.1	152.6	124.9	145.3

Table 8. STAR-CCM+ Porous Predictions vs. Measured Data (°C)

Assembly	2 (3K7)	6 (30A)	14 (57A)	19 (3U9)	24 (3U4)	28 (3U6)	31 (5T9)
Lance positions (in.)							
9	1.7	0.8	-1.9	0.0	2.4	15.0	2.0
25	9.4	12.0	7.0	9.5	11.4	21.7	11.8
40	14.7	16.2	14.4	13.5	11.1	21.7	9.3
60	14.9	15.5	14.1	17.9	10.8	19.7	8.3
76	14.7	14.5	14.7	19.2	11.2	16.4	7.2
94	10.9	12.2	13.4	11.7	5.0	15.9	5.6
117	9.8	7.3	8.4	9.7	6.8	14.6	-1.9
140	7.0	7.2	8.8	13.6	7.1	11.2	2.7
150	-7.4	-2.6	5.1	7.7	-2.8	-5.9	-5.4

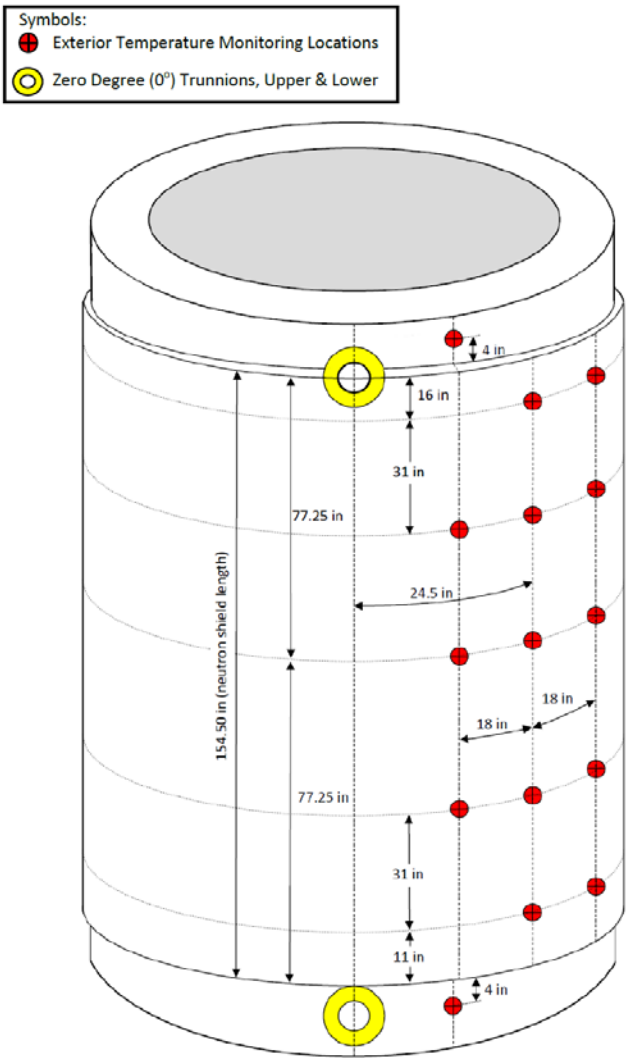

Figure 6. Location of Cask Wall Measurements

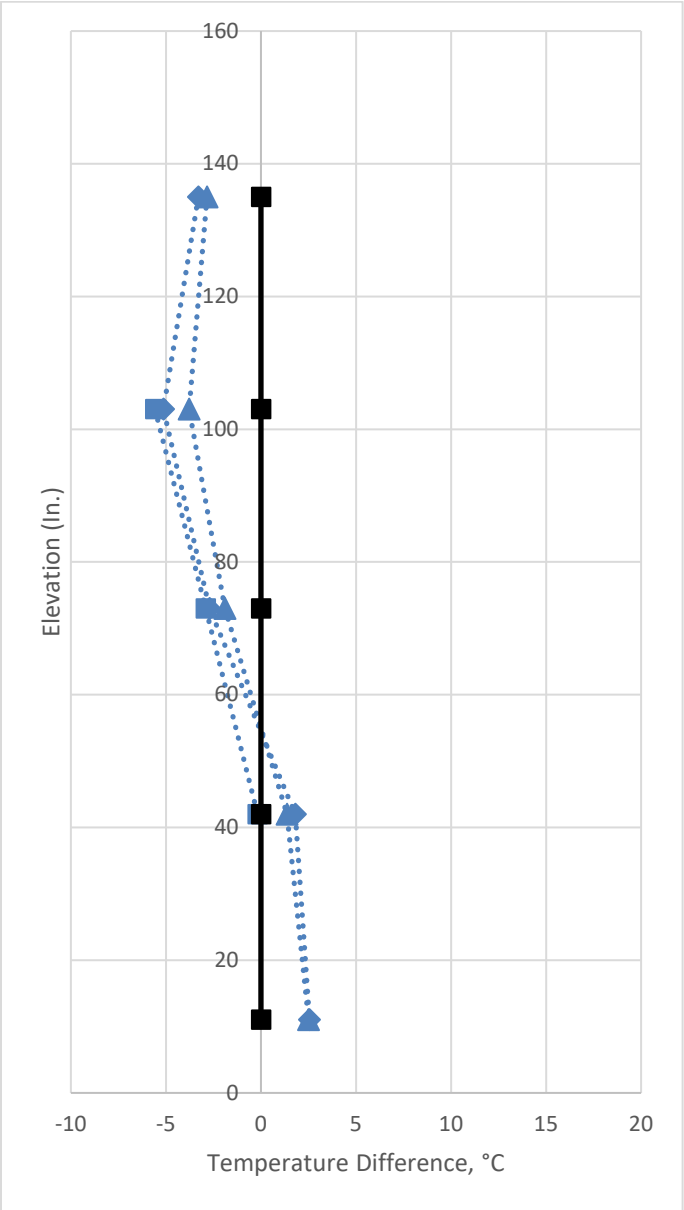

Figure 7. STAR-CCM+ Porous Model – Differences Between Predictions and Cask Surface Temperature Measurements

4.2 STAR-CCM+ Detailed Model

Results for the STAR-CCM+ detailed model are presented in similar fashion to those for the porous model in Section 4.1, with the exception that fewer thermocouple lances can be represented. The one-eighth section model of the cask includes the lance in the hottest basket location, assembly 14, and represents assemblies 2 and 28 by symmetry as shown in Figure 8. Model results for measurement locations for all thermocouple lances are shown in Figure 9. Differences from measurements are shown in Figure 10.

For the thermocouple lances represented in the detailed model, predictions are very close to those from the porous model at the top of the thermocouple lance, but temperatures are higher through the rest of the points. At the bottom, over predictions are greatest, ranging from 17 to 27°C. The generally higher

temperatures are caused, at least in part, by the fact that this eighth section of the cask loading is 2% higher than the average. Also, there is an assembly in the full cask loading across the symmetry plane from the hottest basket location that has only 2/3 of the decay heat (compare assemblies 14 and 20 in Figure 3).

Another difference that impacts the temperature profile at the bottom of the cask is the more accurate treatment of the bottom fuel spacer and its contact with the cask bottom. In the porous model that spacer is represented by a homogeneous material with porosity weighted thermal conductivity. Zircalloy properties are used for the solid fraction and helium for the gas. In both models, perfect contact is assumed with the cask cavity base. In the detailed model that contact is more accurately represented, through the corners of the fuel assembly spacer.

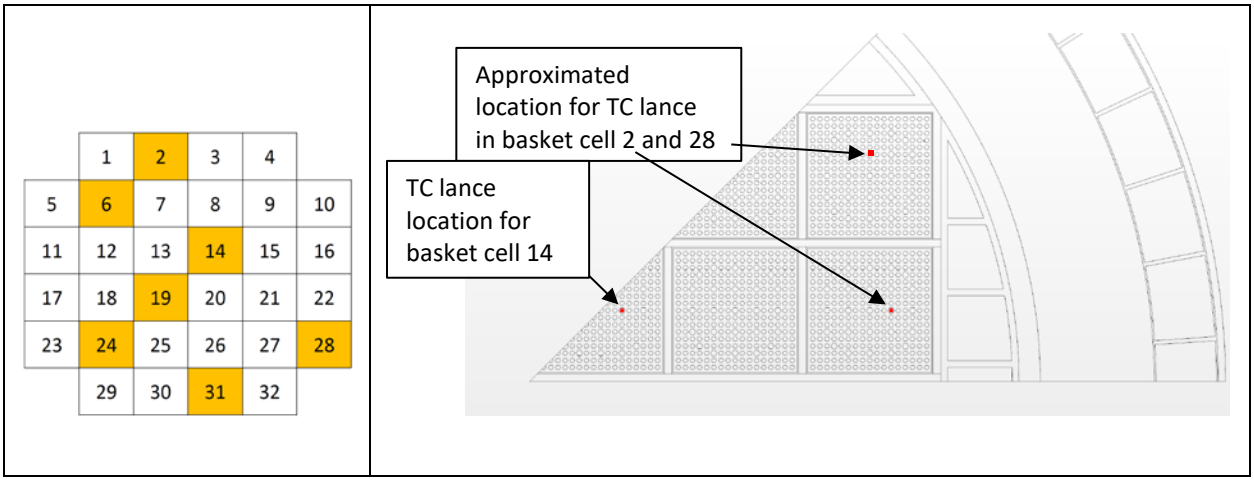

Figure 8. Location of Thermocouple Lances in STAR-CCM+ Detailed Model

Comparisons with cask surface temperatures are shown in Figure 11. Only the first two columns of measurements can be represented by the one-eighth section. The trend in differences from measurements for those locations is consistent with those from the porous model. Results from the detailed model are slightly better, being within +/- 7°F, whereas the porous model was between -10 to +5°F.

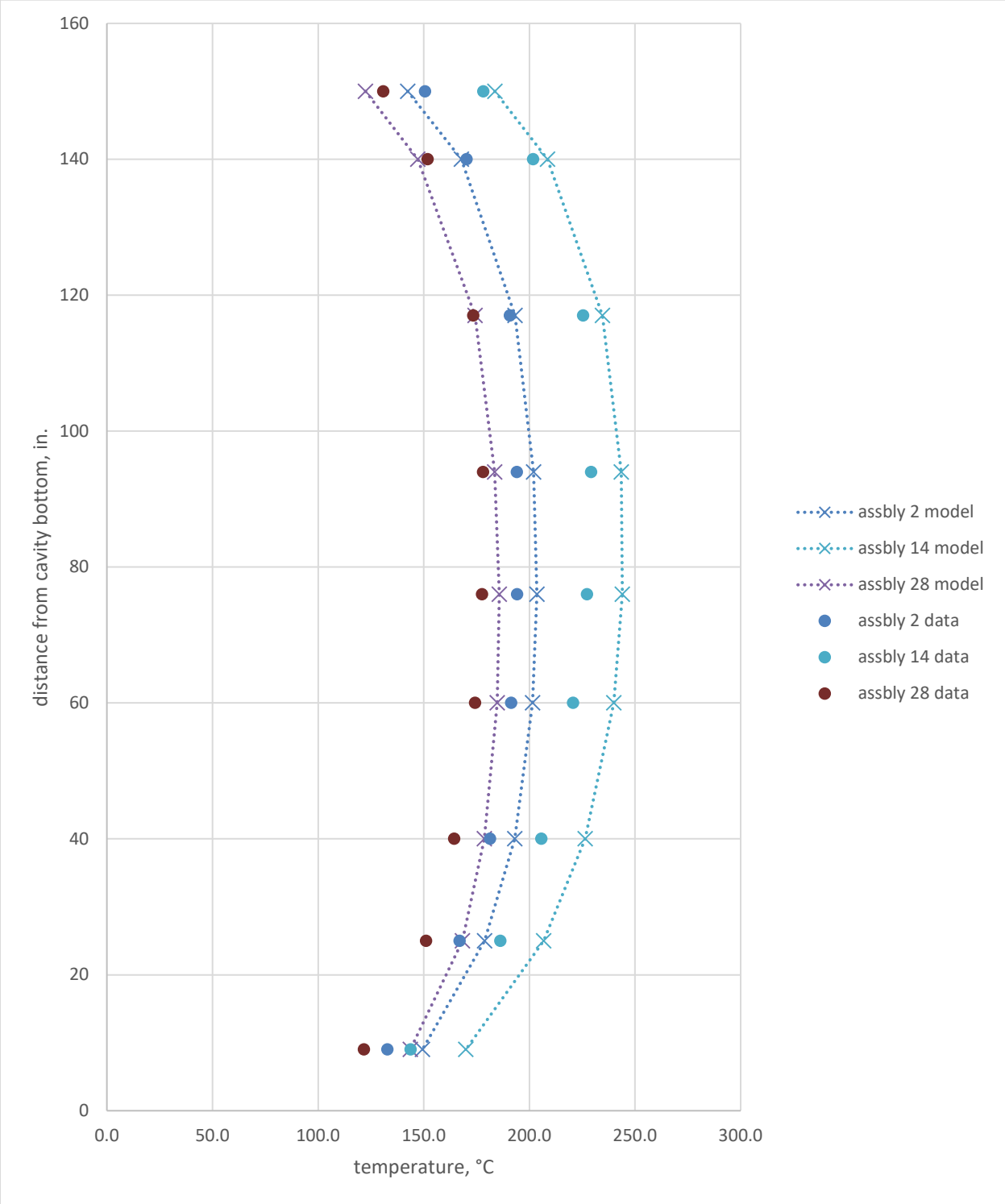

Figure 9. STAR-CCM+ Detailed Model Predictions Compared to Thermocouple Measurements

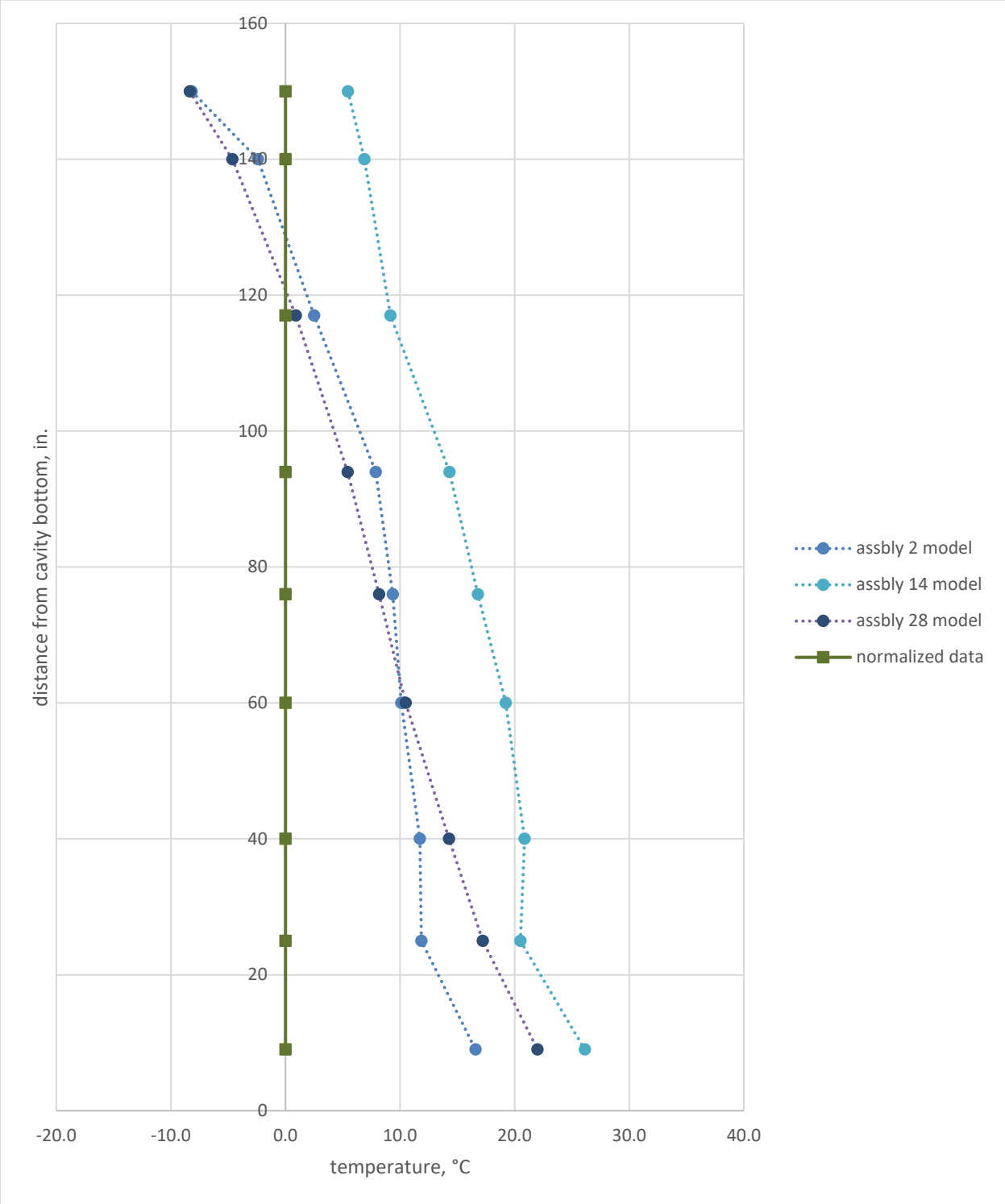

Figure 10. STAR-CCM+ Detailed Model – Differences Between Predictions and Thermocouple Measurements

Table 9. STAR-CCM+ Detailed Thermocouple Predictions (°C)

Assembly	2 (3K7)	14 (57A)	28 (3U6)
Lance positions (in.)			
9	149.4	169.9	143.6
25	178.8	206.7	168.3
40	193.0	226.5	178.7
60	201.5	239.9	184.8
76	203.6	244.0	185.8
94	202.0	243.5	183.5
117	193.2	234.6	174.3
140	167.8	208.6	147.2
150	142.4	183.7	122.4

Table 10. STAR-CCM+ Detailed Predictions vs. Measured Data (°C)

Assembly	2 (3K7)	14 (57A)	28 (3U6)
Lance positions (in.)			
9	16.6	26.1	22.0
25	11.9	20.5	17.2
40	11.7	20.9	14.3
60	10.1	19.2	10.5
76	9.4	16.8	8.2
94	7.9	14.3	5.4
117	2.5	9.2	0.9
140	-2.4	6.9	-4.6
150	-8.2	5.5	-8.4

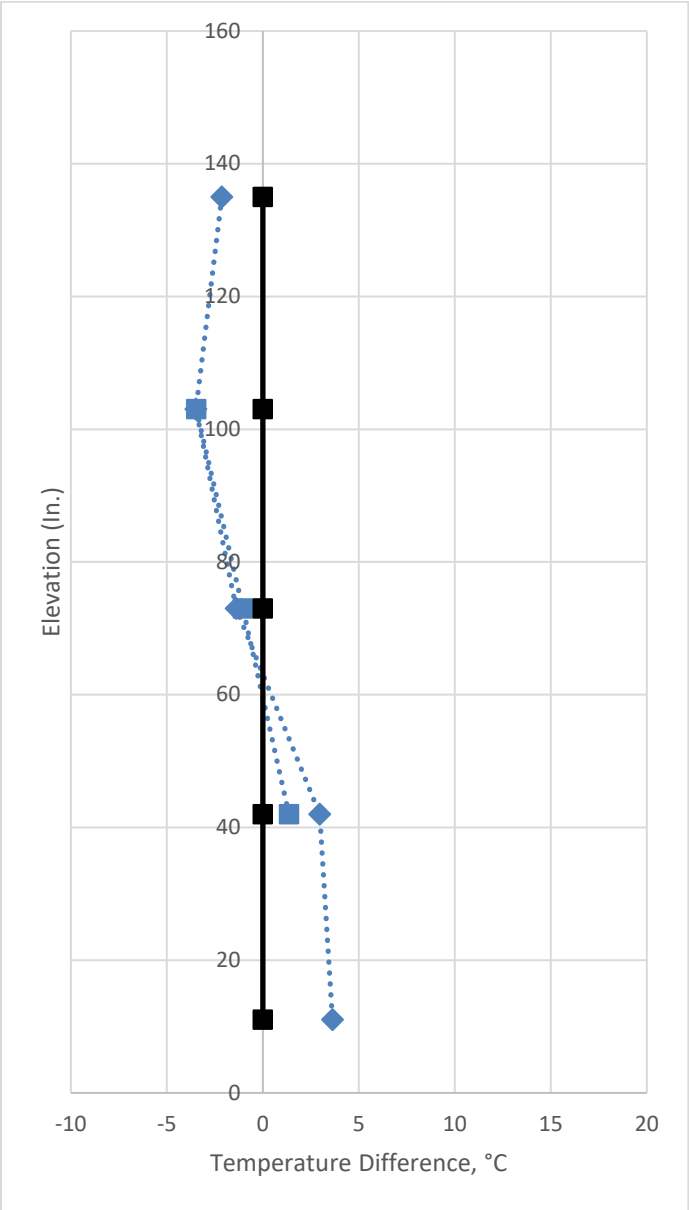

Figure 11. STAR-CCM+ Detailed Model – Differences Between Predictions and Cask Surface Temperature Measurements

4.3 COBRA-SFS Model

This section presents the results from the COBRA-SFS model compared to thermocouple data. Model predictions are compared to measured temperatures in Figure 12 and differences between predictions and measurements are shown in Figure 13. These data are shown in tabular form in Table 11 and Table 12.

For the majority of the measured thermocouple comparisons, the difference between the present results and the initial round robin predictions is <5°C. This is favorable for the purposes of this exercise. Compared to the STAR-CCM+ model, there is still some discrepancy in the prediction of assembly 28. This is likely due to complex recirculation patterns that COBRA-SFS does not predict and is discussed further in Fort et. al 2019a.

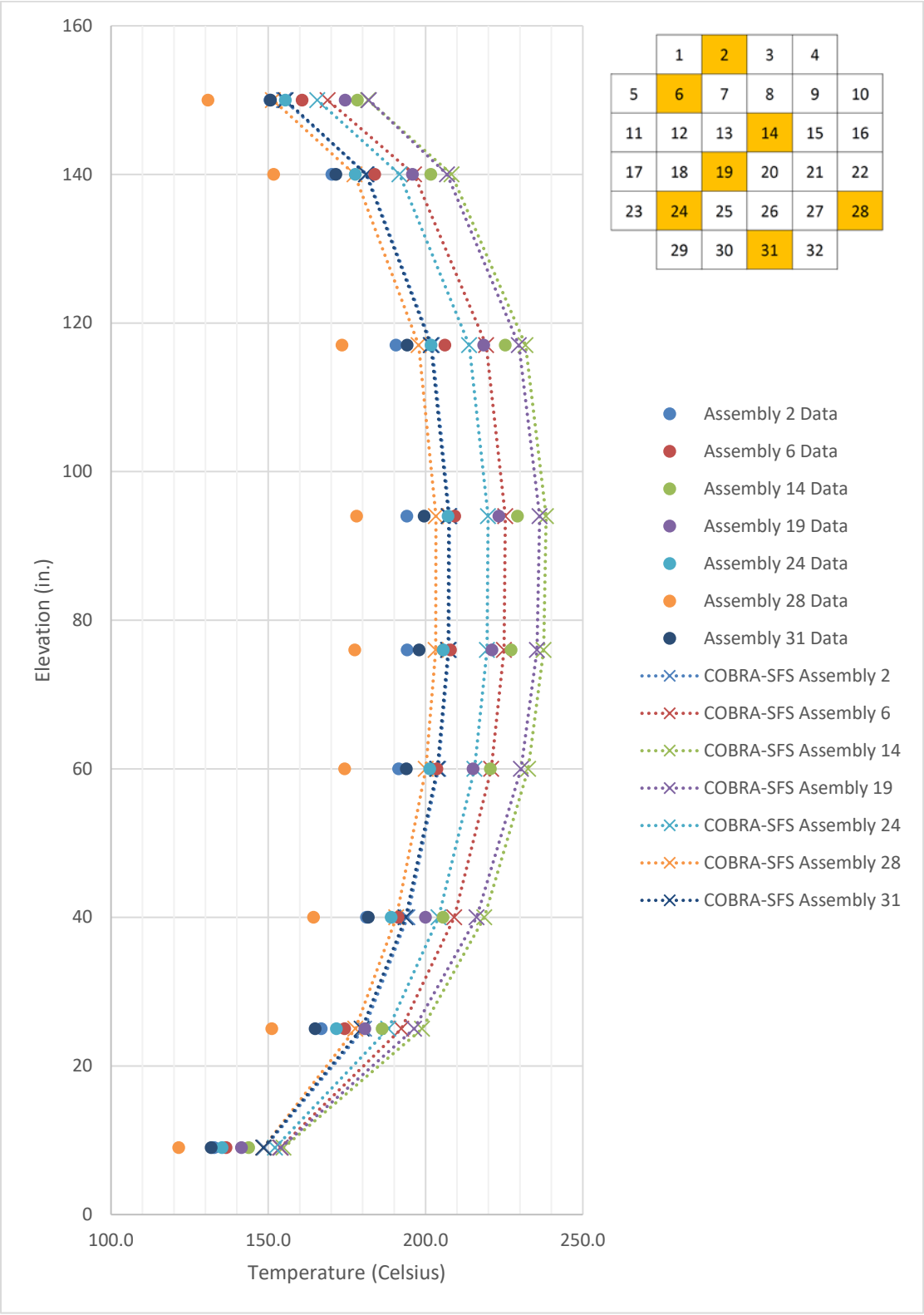

Figure 12. COBRA-SFS Predictions Compared to Thermocouple Measurements

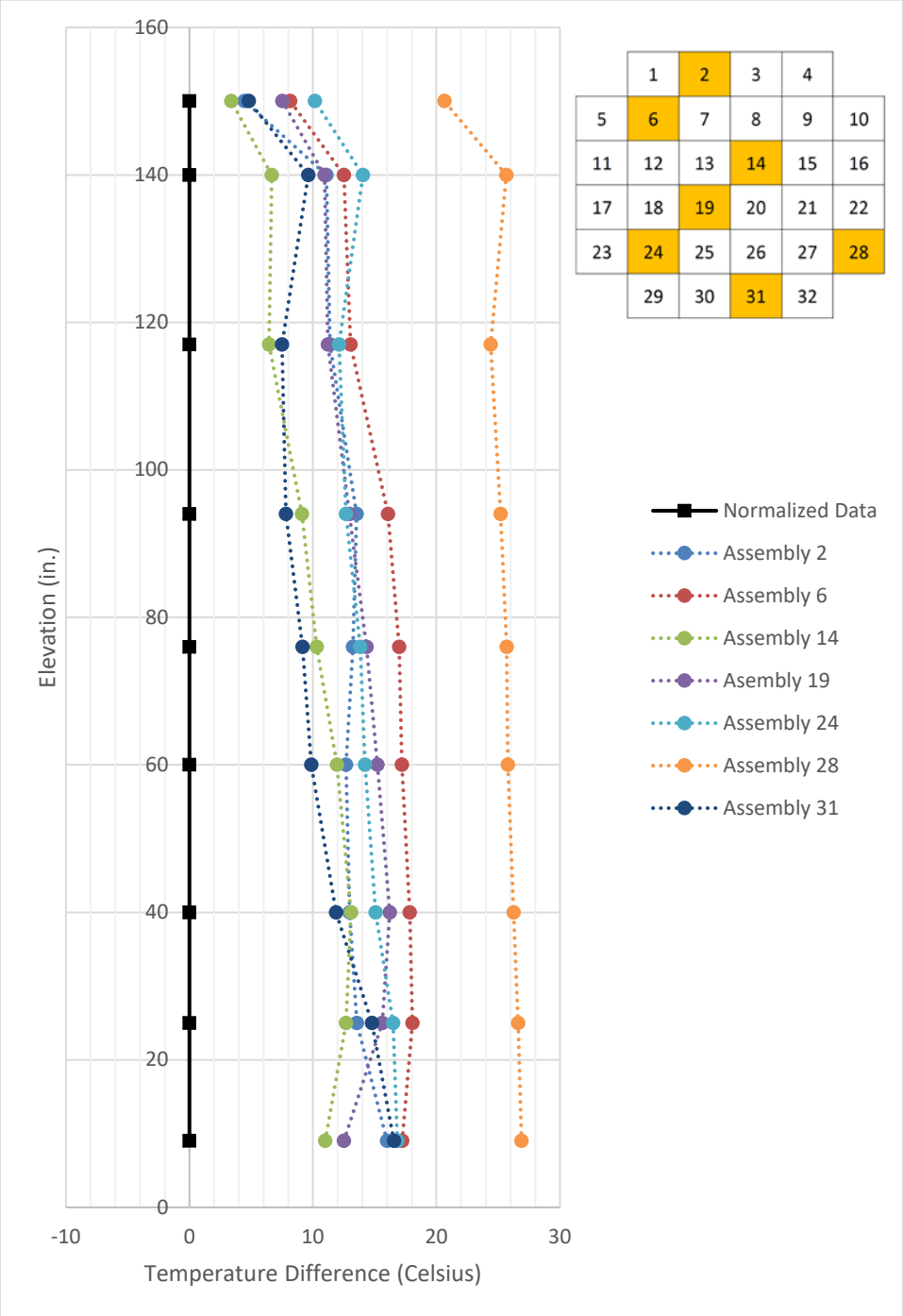

Figure 13. COBRA-SFS Model – Differences Between Predictions and Thermocouple Measurements

Table 11. COBRA-SFS Thermocouple Predictions (°C)

Assembly	2 (3K7)	6 (30A)	14 (57A)	19 (3U9)	24 (3U4)	28 (3U6)	31 (5T9)
Lance positions (in.)							
9	148.8	153.8	154.8	154.0	152.2	148.4	148.4
25	180.4	192.3	198.9	196.4	188.2	177.7	179.7
40	194.3	209.1	218.7	216.2	204.2	190.7	193.7
60	204.1	220.9	232.6	230.4	215.6	200.1	203.8
76	207.5	224.9	237.5	235.4	219.5	203.3	207.2
94	207.6	225.4	238.3	236.3	219.9	203.3	207.4
117	202.1	219.3	231.8	229.7	213.9	197.8	201.7
140	181.3	196.4	208.3	206.8	191.7	177.4	181.1
150	155.0	168.9	181.7	182.0	165.6	151.5	155.5

Table 12. COBRA-SFS Predictions vs. Measured Data (°C)

Assembly	2 (3K7)	6 (30A)	14 (57A)	19 (3U9)	24 (3U4)	28 (3U6)	31 (5T9)
Lance positions (in.)							
9	16.0	17.2	11.0	12.5	16.8	26.9	16.6
25	13.6	18.1	12.7	15.6	16.5	26.6	14.8
40	13.0	17.8	13.1	16.2	15.1	26.3	11.9
60	12.7	17.2	11.9	15.2	14.2	25.8	9.9
76	13.3	17.0	10.3	14.3	13.8	25.7	9.2
94	13.5	16.1	9.1	12.9	12.7	25.2	7.8
117	11.4	13.1	6.4	11.2	12.1	24.4	7.5
140	11.1	12.5	6.7	10.9	14.1	25.7	9.6
150	4.5	8.2	3.4	7.5	10.2	20.6	4.8

COBRA-SFS model results are compared with measured cask surface temperatures in Figure 14. Single values for model results represent average cask surface temperatures at that axial level.

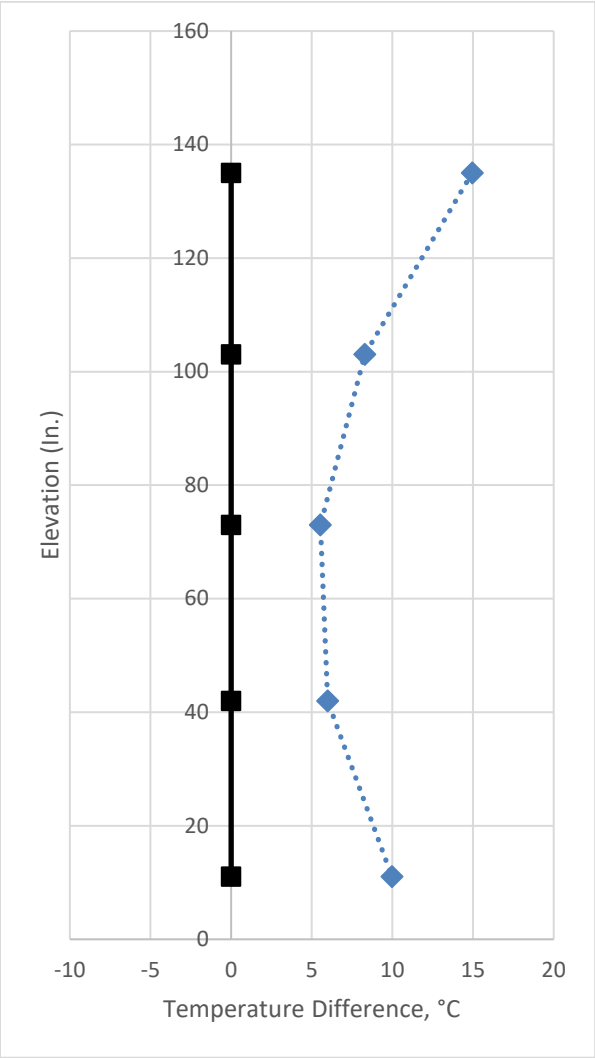

Figure 14. COBRA-SFS Model – Differences Between Predictions and Cask Surface Temperature Measurements

5. CONCLUSIONS

The purpose of the work described in this report was to update preexisting models for the TN-32B demonstration cask with the specifications for the international round robin and determine how well they match the high burnup demonstration project data. The results presented in this report show that all three models compare favorably with the TN-32B demo cask data and with previous model predictions reported by PNNL (Fort et al 2019a). Prediction of thermocouple temperatures was improved with the updated STAR-CCM+ porous model. This was due to the combined changes and resulted in reduction of thermocouple temperatures by at least 7°C. Results from the STAR-CCM+ detailed model, which used an explicit representation of the fuel, were consistent with the porous model in peak values, but agreed less well with measurements at the lower thermocouple positions. Although the COBRA-SFS model boundary conditions have changed significantly, there is a minimal effect on the predicted thermocouple temperatures. An increase of approximately 5°C was observed relative to the previous predictions. The consistency of the predictions from all three models indicate that the International Benchmark specifications will result in favorable predictions against the data collected in the high burnup demonstration cask project. The models predicted well and show only marginally different results from the original modeling, which used proprietary information.

THIS PAGE INTENTIONALLY LEFT BLANK.

6. REFERENCES

DOE. 1981. ET-47912-3. Domestic Light Water Fuel Design Evolution. Vol. 3. Nuclear Assurance Corporation, Atlanta, GA.

DOE. 1992. RW-0184 Rev. 1. Characteristics of Potential Repository Wastes. Volume 1. U.S. Department of Energy, Office of Civilian Radioactive Waste Management.

EPRI. 2014. *High Burnup Dry Storage Cask Research and Development Project – Final Test Plan*. Contract No. DE-NE-0000593, Electric Power Research Institute, Palo Alto, California.

EPRI. 2019. *High Burnup Demo Data. Initial Report – Decon Bay – 11-15-2017 to 11-29-2017*. https://www.epri.com/#/portfolio/2020/research_areas/2/061149?lang=en-US.

EPRI. 2020a. *High-Burnup Used Fuel Dry Storage System Thermal Modeling Benchmark – Round Robin Results*. EPRI report no. 3002013124. Electric Power Research Institute, Palo Alto, California.

EPRI. 2020b. *International Thermal Modeling Benchmark for High-Burnup Used Fuel Dry Storage System: Extended Storage Collaboration Program Activity*. EPRI report no. 3002018498. Electric Power Research Institute, Palo Alto, California.

Fort, JA, TE Michener SR Suffield DJ Richmond. 2016. *Thermal Modeling of a Loaded MAGNASTOR Storage System at Catawba Nuclear Station*. PNNL-25871. Pacific Northwest National Laboratory, Richland, Washington.

Fort, JA, DJ Richmond, JM Cuta and SR Suffield. 2019a. *Thermal Modeling of the TN-32B Cask for the High Burnup Spent Fuel Data Project*. PNNL-28915, Pacific Northwest National Laboratory, Richland, Washington.

Fort, JA, DJ Richmond, BJ Jensen and SR Suffield. 2019b. *High Burnup Demonstration: Thermal Modeling of TN-32B Vacuum Drying and ISFSI Transients*. PNNL-29058. Pacific Northwest National Laboratory, Richland, Washington.

Holman, J P. 1996. *Heat Transfer*, McGraw Hill, NY.

Incropera, FP, DP Dewitt, TL Bergman, AS Lavine, *Fundamentals of Heat and Mass Transfer*, Fifth Edition, John Wiley and Sons, 2007.

Michener TE, DR Rector, JM Cuta, and HE Adkins, Jr. 2017. *COBRA-SFS: A Thermal-Hydraulic Code for Spent Fuel Storage and Transportation asks, Cycle 4a.* PNNL-24841, Pacific Northwest National Laboratory, Richland, Washington.

Siemens, PLM. 2020. STAR-CCM+ 15.02 (computer software). Siemens Product Lifecycle Management Software, Inc., Plano, Texas.